Dramatic modulation of electron transfer in protein complexes by crosslinking

Amsterdam, I.M.C. van; Ubbink, M.; Einsle, O.; Messerschmidt, A.; Merli, A.; Cavazzini, D.; ... ; Canters, G.W.

Citation
Amsterdam, I. M. C. van, Ubbink, M., Einsle, O., Messerschmidt, A., Merli, A., Cavazzini, D., ... Canters, G. W. (2001). Dramatic modulation of electron transfer in protein complexes by crosslinking. *Nature Structural Biology*, *9*(1), 48-52. doi:10.1038/nsb736

Version:	Publisher's Version
License:	Licensed under Article 25fa Copyright Act/Law (Amendment Taverne)
Downloaded from:	https://hdl.handle.net/1887/3608255

Note: To cite this publication please use the final published version (if applicable).

Dramatic modulation of electron transfer in protein complexes by crosslinking

Irene M. C. van Amsterdam[1], Marcellus Ubbink[1], Oliver Einsle[2], Albrecht Messerschmidt[2], Angelo Merli[3], Davide Cavazzini[3], Gian Luigi Rossi[3] and Gerard W. Canters[1]

[1]*Leiden Institute of Chemistry, Gorlaeus Laboratories, Leiden University, P.O. Box 9502, 2300 RA Leiden, the Netherlands.* [2]*Max-Planck-Institut für Biochemie, Abteilung Strukturforschung, Am Klopferspitz 18a, 82152 Martinsried, Germany.* [3]*Istituto di Scienze Biochimiche, Università degli studi di Parma, Parco della Scienze 23A, 43100 Parma, Italy.*

Published online: 10 December 2001, DOI: 10.1038/nsb736

© 2002 Nature Publishing Group http://structbio.nature.com

The transfer of electrons between proteins is an essential step in biological energy production. Two protein redox partners are often artificially crosslinked to investigate the poorly understood mechanism by which they interact. To better understand the effect of crosslinking on electron transfer rates, we have constructed dimers of azurin by crosslinking the monomers. The measured electron exchange rates, combined with crystal structures of the dimers, demonstrate that the length of the linker can have a dramatic effect on the structure of the dimer and the electron transfer rate. The presence of ordered water molecules in the protein–protein interface may considerably influence the electronic coupling between redox centers.

The transfer of electrons between protein redox partners in the living cell depends on the formation of short-lived protein complexes, whose turnover must be sufficiently high in order not to limit the overall rate of energy production. In addition, complex formation must be specific so that redox equivalents are not wasted in chance encounters, effectively short circuiting the cellular machinery. How the noncovalent forces that govern complex formation are tuned to produce both the right specificity and the right affinity is not well understood[1–5]. Although chemical crosslinking has been applied to 'freeze' the complexes in order to make them amenable to analysis, this often reduces or even abolishes electron transfer[6–9]. To shed new light on this problem, we have analyzed the effect of crosslinking on the electron transfer between molecules of azurin, a small 14 kDa blue copper protein from *Pseudomonas aeruginosa*.

In the crystal of wild type native azurin, the protein molecules pack as noncovalent dimers with their 'hydrophobic patches' opposite each other (Fig. 1*a*,*b*)[10,11]. Although there is no evidence of dimer formation in solution, this orientation has been suggested to be similar to the transient complex that is formed in solution during the electron self-exchange (e.s.e.) reaction[12,13]. In this reaction, an electron is exchanged between a reduced and an oxidized azurin molecule. Inspection of the structure shows that the Asn 42 residues of the two molecules in this dimer are in close proximity (Fig. 1*a*). By computer replacement of Asn 42 with Cys, building a strain-free model in which a disulfide bridge connects the monomers is possible. Inspired by this finding, we constructed the N42C mutant and succeeded in forming dimers of azurin that are crosslinked *via* the Cys 42-S–S-Cys 42 disulfide bridge (SSdim)[14]. We also linked the Cys 42 sulfurs *via* a bifunctional symmetric linker, *bis*-maleimidomethylether (BMME), creating a Cys 42-S–BMME–S-Cys 42 crosslink (BMMEdim). The electron transfer rates between Cu^{I} and Cu^{II} within, as well as between, the dimers were measured and analyzed as follows.

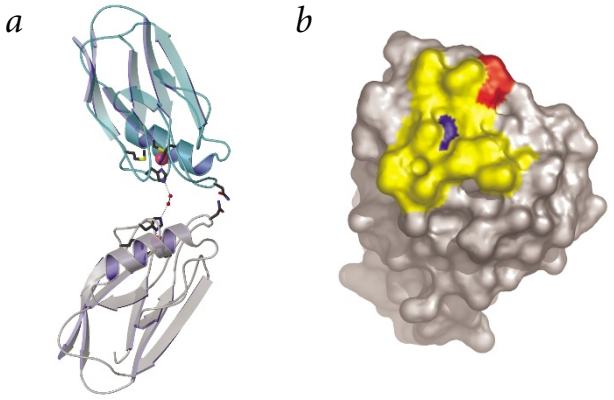

Fig. 1 Wild type azurin. ***a***, Ribbon diagram of noncovalent dimer complex of wild type azurin as observed in asymmetric unit (PDB entry 4AZU). Coppers are depicted as magenta spheres. Side chains of copper ligands and residue 42 are displayed, with C, O, N and S depicted in black, red, blue and yellow, respectively. Two monomers face each other, with their hydrophobic patches opposing as in (*b*). Two water molecules in the interface connect the copper ligands His 117 *via* hydrogen bonds. The distance between the coppers is 14.7 Å. This image and Fig. 3 were generated with MOLSCRIPT[27], BOBSCRIPT[28] and RASTER3D[29]. ***b***, Molecular surface representation of wild type azurin showing the position of the hydrophobic patch (yellow) surrounding the copper ligand His 117 (blue) and the position of Asn 42 (red). The molecule is slightly tilted relative to the orientation of the gray monomer in (*a*). The map was prepared with PyMOL[30].

Electron self-exchange

In the proton NMR spectrum of native azurin, the resonances of the methyl groups of Val 31 are sensitive to the redox state of the protein[15]. The resonance of one of the methyl peaks shifts from –0.68 to –0.74 p.p.m. upon oxidation of the copper. In a mixture of Cu^{I} and Cu^{II} wild type azurin, the resonance position is the weighted average of both forms because the e.s.e. rate is much faster than the frequency difference at 14.1 T ('fast exchange' condition) (Fig. 2*a*). In SSdim, the same shift pattern "as wild type" is observed (Fig. 2*b*). In contrast, the resonances of the Cu^{I} and Cu^{II} species of BMMEdim do not shift but change intensity in agreement with the ratio of Cu^{I} and Cu^{II} azurin, showing that the intermolecular exchange is slow. Furthermore, a third resonance, whose position is independent of the ratio of Cu^{I} and Cu^{II} azurin, is observed precisely in between these resonances (Fig. 2*c*). This third resonance represents the population of dimers that are half-oxidized (Cu^{I} / Cu^{II}). Within such a dimer, the unpaired electron exchanges fast between the coppers (intramolecular electron transfer). The concentration of half-oxidized dimers is expected to be maximal in a 50% oxidized sample, with a 1:2:1 ratio for reduced:half oxidized:oxidized dimers, which agrees with the resonances at 51% (Fig. 2*c*). The assignment of the middle resonance to half-oxidized dimers is confirmed by the NMR spectrum of a heterodimer containing one copper and one zinc ion; in this case, the intramolecular electron transfer is absent because Zn^{II} is not redox active. For this dimer, the resonances of the Val 31 methyl in Cu^{I} and Zn^{II} azurin (both at –0.67 p.p.m.) and Cu^{II} azurin (–0.73 p.p.m.) can be distinguished, but the intermediate resonance is absent (Fig. 2*d*).

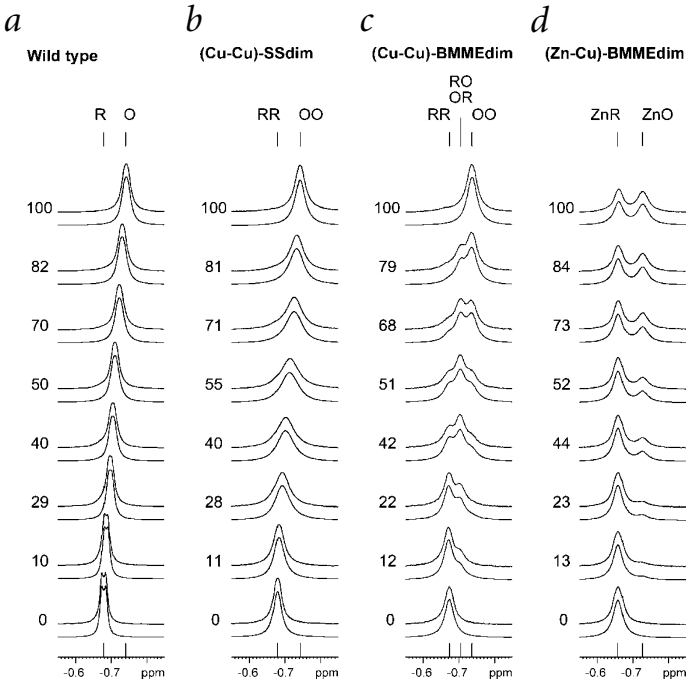

Fig. 2 Region of the ^{1}H NMR spectra showing the Val 31 methyl signal (—0.7 p.p.m.) as a function of the percentage of oxidized protein. Experimental data are shown in the upper traces; simulated spectra generated using MEX/MEXICO[16] are shown in bottom traces. ***a***, Wild type azurin. R and O denote the position of the Val 31 methyl signal of the reduced and oxidized monomer, respectively. ***b***, (Cu-Cu)-N42C SSdim. RR and OO denote the position of the Val 31 methyl signals of the fully reduced and fully oxidized dimer, respectively. ***c***, (Cu-Cu)-N42C BMMEdim. RR and OO indicate the position of the Val 31 signals of fully reduced and oxidized dimer, respectively. RO and OR represent the position of the Val 31 signal of half-reduced/half-oxidized dimers in which electron exchange is fast. ***d***, (Zn-Cu)-N42C BMME dimer. The positions of the Val 31 resonance in the reduced and oxidized (Zn-Cu) BMMEdim are represented by ZnR and ZnO, respectively. The Val 31 signal of the Zn^{II} azurin coincides with the one for Cu^{I} azurin. The slight increase in width of the signals of the dimers in (*b*–*d*) compared to the wild type monomer (*a*) is due to the larger rotational correlation time of the dimers.

The experimental NMR traces were simulated using MEX/MEXICO[16] (bottom traces, Fig. 2) to derive values for both the intra- and intermolecular electron exchange rates (Table 1). The simulations include the effects of scalar coupling that are visible in the reduced form of wild type azurin (Fig. 2*a*), increased relaxation in the oxidized protein and the additional line broadening observed in dimers due to larger rotational correlation times, as well as the various types of exchange expected. The intermolecular electron self-exchange rate constants are also deduced from the NMR line broadening of the His 46 Cδ2 proton resonance at 5.89 p.p.m. as a function of the percentage oxidized protein[14] (Table 1).

The intramolecular electron transfer is very slow in SSdim, with an upper limit of 10 s^{-1} (ref. 14), and very fast in BMMEdim, with a lower limit of 5×10^4 s^{-1}. Also, intermolecular electron transfer between dimers is fast for the SSdim, with $k_{inter} = 4.2 \times 10^5$ M^{-1} s^{-1}, which is about seven times slower than for wild type azurin[14], and slow for the BMMEdim, with the e.s.e. at least 300× slower than wild type azurin (Table 1).

Crystal structures

SSdim and BMMEdim were crystallized in order to determine their structures and compare them with the noncovalent dimer observed for wild type azurin in crystals (Fig. 1*a*). The crystal structure of SSdim (Fig. 3*a*) shows that the monomers have rotated away from each other, exposing the hydrophobic patches and resulting in an intradimer copper-to-copper distance of 25.9 Å. One monomer of each dimer has an extensive contact area with a monomer of another dimer, with an interdimer Cu-Cu distance of 15.1 Å (Fig. 3*b*). This orientation is similar, although not identical, to that in the crystals of wild type azurin. The buried surface area between the two interacting monomers in the SSdim is 956 ± 7 $Å^2$ (averaged over three dimer interfaces in the asymmetric unit) of mainly hydrophobic residues. No ordered water molecules were detected in the interface. In contrast, the structure of BMMEdim (Fig. 3*c*) shows a structure similar to the noncovalent dimer of wild type azurin, with an intradimer copper-to-copper distance of 14.6 Å and two water molecules connecting the copper ligands His 117 with each other *via* three hydrogen bonds (Fig. 3*c*,*d*). The surrounding protein–protein interface is of hydrophobic nature, with 11 residues in van der Waals contact with the other monomer. The outer edge of the interface, including the BMME, is polar, with an additional bridging water molecule between the backbone oxygen atoms of Cys 42 in both monomers. The buried surface area in the interface is 1,136 $Å^2$, and the dimer is fully symmetric.

Thus, contrary to our initial expectation, the dimer with the short crosslink does not exhibit fast intramolecular electron transfer in solution. Apparently the Cys 42-Cys 42 link is too tight to allow the hydrophobic patches to come in close contact without causing steric hindrance. The hydrophobic forces that promote formation of a transient electron transfer complex are weaker than the forces that hold together the tertiary structure of the protein. Even a small rearrangement of the loop around Cys 42 (residues 36–47) does not take place, preventing the interaction of the hydrophobic patches. The fast intermolecular e.s.e. confirms that the hydrophobic patches in SSdim do not interact strongly but, instead, are still available for the reaction with other dimers. The crystal structure of this dimer (Fig. 3*a*,*b*) supports these results. The small increase in copper-to-copper distance and the slightly diminished accessibility of the hydrophobic patch of one monomer, because of the presence of the covalently linked second monomer, contribute to the sevenfold decrease in intermolecular e.s.e. rate compared to wild type azurin.

The introduction of a longer crosslink (BMME) allows the formation of an azurin dimer in solution, in which fast intramolecular electron transfer occurs. The very low intermolecular e.s.e. rate of BMMEdim suggests that its hydrophobic patches interact strongly, prohibiting fast electron transfer between dimers. This agrees with the crystal structure, in which both hydrophobic patches are part of the dimer interface, making them unavailable for e.s.e. between dimers. Thus, the crystal structure can be assumed to be representative of the structure in solution and can be used to compare our kinetic results with electron transfer theory.

© 2002 Nature Publishing Group http://structbio.nature.com

© 2002 Nature Publishing Group http://structbio.nature.com

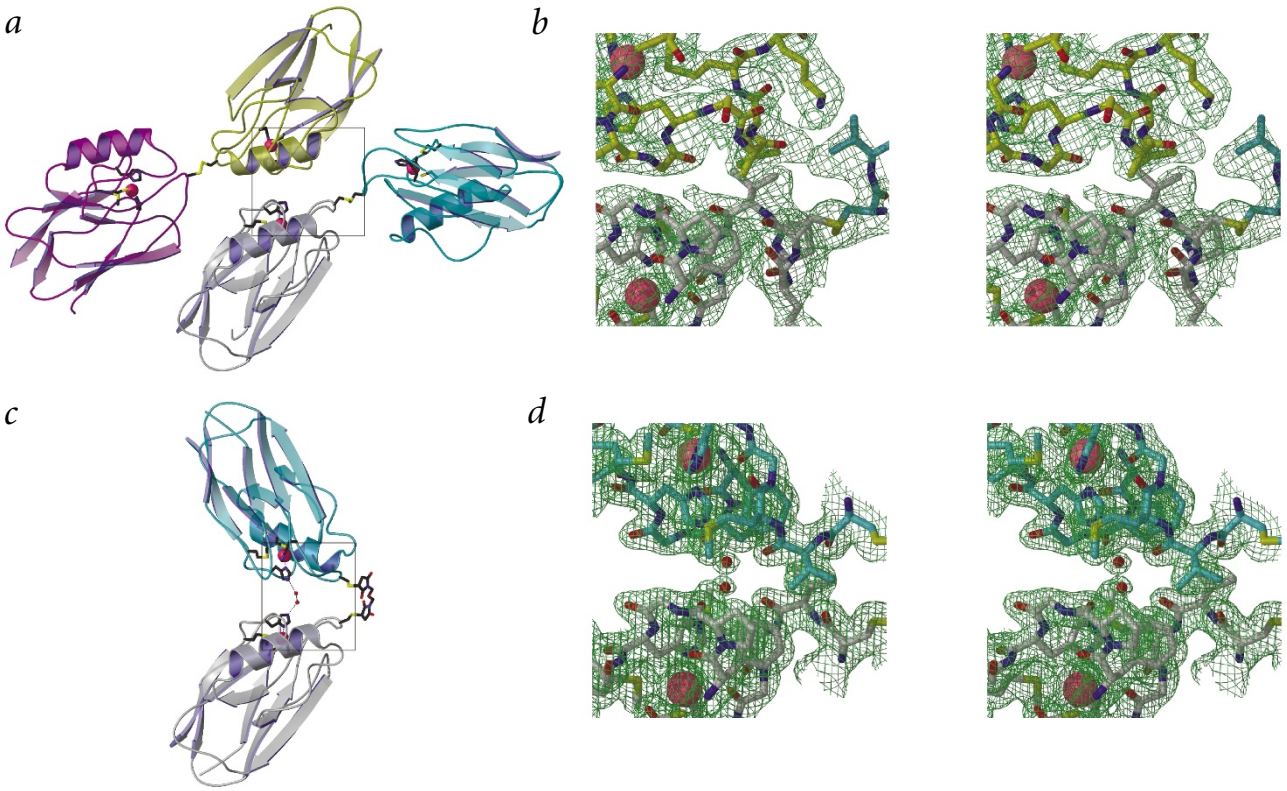

Fig. 3 Crystal structures of N42C azurin dimers. ***a***, Ribbon diagram of SSdim as observed in the asymmetric unit: four monomers are arranged in two crosslinked dimers. As a reference, the gray monomer is in a similar orientation as Fig. 1*a*. The monomers in the crosslinked dimers have rotated away from each other, exposing the hydrophobic patches, which results in an intradimer Cu-to-Cu distance of 25.9 ± 0.3 Å (average and error margin from six dimers in the asymmetric unit). The interdimer Cu-to-Cu distance equals 15.1 ± 0.1 Å. ***b***, Stereo view showing the experimental electron density map of the region (indicated by a box in (*a*)) involved in interaction between two SSdim molecules (residues 40–45 and 114–117 of the gray monomer (chain I) and residues 114–122 of the yellow monomer (chain L) are shown). The disulfide bridge connecting the gray monomer (chain I) to its partner (blue monomer, chain J) is shown as well (residues 42 and 43 of blue monomer are displayed). The electron density is superimposed on the refined model and contoured at 1 σ. ***c***, Ribbon diagram of BMMEdim showing the great similarity with the noncovalent wild type azurin dimer complex (Fig 1*a*). As a reference the gray monomer is in a similar orientation as Fig 1*a*. BMME is shown color-coded as described in Fig. 1*a*. The two monomers pack with their hydrophobic patches facing each other, with a Cu-to-Cu distance of 14.6 Å. Two water molecules in the interface connect the His 117 residues through hydrogen bonding. ***d***. Stereo view showing the experimental electron density map of the region (indicated by a box in (*c*)) involved in interaction between two monomers in BMME-linked dimers (residues 42–46, 114–118 and 121 of both monomers A (gray) and B (blue) are shown). The electron density is superimposed on the refined model and contoured at 1σ.

Comparison with electron transfer theory

Currently there are two types of models to analyze electron transfer rates. The first model, the phenomenological model of Dutton and co-workers, relates the rate of electron transfer to the distance between redox centers[17]. In the second model, the pathway model, Beratan and Onuchic provide a semiempirical model to calculate the electronic coupling between redox centers[18]. In the following we apply both models to our data.

The Dutton model[17] predicts that electron transfer rates (k_{et}) will vary exponentially with the distance (R) separating the redox cofactors and with the packing density of the protein (ρ) in the region between redox sites:

$$\log k_{et} = 13.0 - (1.2 - 0.8\rho)(R - 3.6) - 3.1(\Delta G + \lambda)^2/\lambda \qquad (1)$$

The free energy ΔG and the reorganization energy λ are expressed in eV. When applying Eq. 1 to the BMMEdim, using a λ value of 0.7 eV (ref. 19), ρ = 0.9, R = 14.6 Å and ΔG = 0 (self-exchange reaction), a value of $k_{et} = 4 \times 10^5$ s^{-1} is obtained. This value agrees with the experimentally determined lower limit of $k_{et} \geq 5 \times 10^4$ s^{-1}. Similarly, we find that SSdim has values of R = 25.9 Å and ρ = 0.75, and a value of $k_{et} = 2.8 \times 10^{-3}$ s^{-1}, which again agrees with the experimentally determined upper limit of $k_{et} \leq 10$ s^{-1}.

The dependence of the rate on the protein structure arises in Eq. 1 through the parameter ρ, which represents the packing density of the protein in between the redox centers and is not very sensitive to the atomic details of the structure. The presence of two ordered water molecules in the interface of the BMMEdim, therefore, is not expected to have a large bearing on the predictions made on the basis of Eq. 1.

The influence of the two water molecules on the electronic coupling between the redox sites in the BMMEdim can also be analyzed by using the model developed by Beratan and Onuchic[18], in which the structural details of the intervening medium determine the long-range couplings. The overall electronic coupling factor, T_{DA}, is specified as the product of the individual couplings between atoms, which can be covalent bonds, hydrogen bonds or through-space jumps. According to this algorithm and using the three-dimensional structure of BMMEdim, an electronic decay factor of $\Pi_\varepsilon = 1.1 \times 10^{-3}$ is calculated for the coupling from copper to copper *via* both His 117 residues and the two water molecules. In the absence of the water molecules at the monomer–monomer interface, the

© 2002 Nature Publishing Group http://structbio.nature.com

Table 1 E.s.e. rate constants of wild type azurin and azurin dimers

	k_{inter} (10^5 $M^{-1}s^{-1}$)		k_{intra} (s^{-1})
	His 46[1]	Val 31[2]	
Wild type monomer	28 ± 5	13 ± 7	n.a.[3]
(Cu-Cu)-N42C SSdim	4.2 ± 0.7	2.8 ± 0.8	≤10 [1]
(Zn-Cu)-N42C SSdim	4.2 ± 1.0	nd[4]	na[3]
(Cu-Cu)-N42C BMMEdim	≤0.2	≤0.06	$\geq 5 \times 10^4$
(Zn-Cu)-N42C BMMEdim	≤0.3	≤0.06	na[3]

[1]Rates were determined by measuring the NMR line broadening of the His 46 Cδ2 proton resonance at 5.89 p.p.m. as a function of the percentage of oxidized protein in a 1 mM solution of azurin[14].
[2]Rates were determined by simulating the proton resonance of the Val 31 methyl group ~–0.7 p.p.m. using MEX/MEXICO[16].
[3]Not applicable.
[4]Not determined.

strongest coupling proceeds *via* the His 117 and one of the Met 13 residues involving two through-space jumps[20] ($\Pi_\varepsilon = 2.0 \times 10^{-6}$). This value is 500× smaller than the former case. The large difference in decay factor illustrates that the participation of water molecules in the electron exchange reaction in this model can make a big difference in the exchange rate[12,21,22].

Conclusions

We have determined that crosslinking with a short linker, even in an apparently optimal position, can impede electron transfer because it may restrict mobility of the partners in the complex with respect to each other. Short linkers, particularly zero-distance linkers, are popular in crosslinking experiments[6–9]. The data presented here clarify why electron transfer is often absent in such crosslinked complexes. The use of a longer, more flexible linker is more appropriate because it allows the partners to sample a large region of configurational space. In this way, complexes may form that are more like the ones formed between the partners free in solution and which are more favorable for electron transfer. This conclusion may also be of interest in the development of biosensors based on redox proteins because the electron transfer rate can be a critical parameter in such systems.

Methods

Construction of dimers. The N42C azurin mutant was constructed and purified as described[14]. Disulfide dimers of the N42C azurin were obtained by adding $Cu(NO_3)_2$ to a solution of the apo form of the protein under air. The construction of BMME-linked dimers of N42C was started by reducing Cu-N42C azurin with 5 mM dithiothreitol (DTT) or a 10-fold molar excess of tris(carboxyethyl)phosphine (TCEP) for at least 1 h at 20 °C in 25 mM potassium phosphate, pH 7. Subsequently, DTT was removed by repeated concentration and dilution using Amicon ultrafiltration equipment. Removing excess TCEP during conjugation with maleimide was not necessary. The protein solution was diluted to a concentration of 0.1 mM, and 0.6 equivalents of BMME (Calbiochem) dissolved in dimethyl sulfoxide (DMSO) were added dropwise to the stirred protein solution (end concentration 0.5% (v/v) DMSO). After stirring at 20 °C for 1 h, the solution was kept overnight at 4 °C. Finally, the solution was concentrated, reduced with 5 mM DTT (to reduce possibly formed disulfide linked dimers) and purified by gel filtration chromatography (Superdex 75, Pharmacia) in the presence of 2 mM DTT. (Zn-Cu)-BMME heterodimers were obtained analogously to the homodimers, except for the starting material that contained a 1:1 mixture of Cu-N42C and Zn-N42C. After gel filtration, the (Zn-Cu)-BMME dimers were separated from the (Cu-Cu) and (Zn-Zn) homodimers by anion exchange chromatography (Q-Sepharose) under reducing conditions.

NMR spectroscopy. NMR experiments were performed on a Bruker Avance DMX 600 MHz spectrometer at 313 K. Free induction decays were accumulated in 16 K memory and Fourier-transformed using a shifted squared sine window function. The chemical shifts were calibrated using 200 μM sodium 3-(trimethylsilyl)propionated$_4$ (TSP) as an internal reference. Samples were typically between 0.3 and 1.0 mM in total protein concentration in D_2O (99.9%) and 25 mM potassium phosphate buffer, pH 8.5 (uncorrected for deuterium isotope effect). Cu^I azurin samples were obtained by reducing Cu^{II} azurin with one equivalent of ascorbic acid, which was subsequently removed by repeated concentration and dilution (Amicon ultrafiltration). Argon was passed through all buffers prior to use to prevent reoxidation. Azurin samples with oxidation grades ranging from 0 to 100% were obtained by mixing the appropriate amounts of reduced and oxidized protein at the same stock concentration. The actual degree of oxidation was determined by measuring the absorbance at 628 nm relative to a fully oxidized sample using a special sample holder that was designed to allow the absorbance to be measured at 628 nm in the NMR tube on a Perkin Elmer lambda 800 spectrophotometer using optical fibers (Hellma).

Simulation of NMR lineshapes. Exchange rates were determined by simulating the NMR lineshapes on an SGI Indy Computer using MEX (for SSdim and BMMEdim) and MEXICO (for wild type azurin)[16], and comparing them visually with the experimental spectra using the dual display features of the spectrometer software (XWINNMR). MEX/MEXICO use an approach based on generalized transition probabilities for dynamic systems[16]. The spectra of wild type azurin were simulated as a case of a two-site exchange that included scalar coupling. The equilibrium constant, needed to define the reverse rate, was given by the experimental ratio between oxidized and reduced azurin. SSdim and Cu-Cu BMMEdim were simulated with an uncoupled exchanging system consisting of four sites — (i) doubly reduced dimer (ii) oxidized half of semireduced dimer (iii) reduced half of semireduced dimer and (iv) doubly oxidized dimer — and four exchange processes, three intermolecular and one intramolecular ((ii) with (iii)). Zn-Cu BMMEdim was simulated with an uncoupled exchanging system consisting of four sites — (i) Cu^I in $ZnCu^I$–dimer; (ii) Zn in $ZnCu^I$–dimer; (iii) Cu^{II} in $ZnCu^{II}$–dimer and (iv) Zn in $ZnCu^{II}$–dimer — and one exchange process ((i) with (iii)). Values for chemical shifts and linewidths of reduced and oxidized signals were taken from

Table 2 Crystallographic statistics

Crystal	N42C BMMEdim	N42C SSdim
Space group	$P6_1$[1]	$P2_12_12_1$
Unit cell (Å)		
a	48.605	86.320
b	48.605	94.425
c	284.809	193.362
Molecules[2] per asymmetric unit	2	12
Resolution range (Å)	50.0 – 2.0	50.0 – 2.75
Independent reflections	22,535	42,605
Completeness[3] (%)	99.5 (99.9)	86.2 (86.4)
R_{merge}[3]	0.070 (0.440)	0.108 (0.484)
$I / \sigma (I)$[3]	15.0 (2.1)	7.1 (1.6)
R_{cryst}	0.190	0.239
R_{free}	0.227	0.293
R.m.s. deviations		
Bonds (Å)	0.0054	0.0093
Angles (°)	1.300	1.340

[1]The true space group of this crystal was $P6_122$, with the BMME linker lying on a crystallographic dyad. In order to be able to build a linked dimer, refinement was carried out in $P6_1$ with strict NCS restraints for the two monomers.
[2]Molecules seen as monomeric azurin subunits.
[3]Numbers in parentheses are for the last shell.

the experimental NMR spectra of the fully reduced and oxidized samples, respectively.

Crystallization and structure determination. Crystals of the SSdim were obtained by sitting drop vapor diffusion, equilibrating a 4 mg ml^{-1} protein solution against a reservoir buffer containing 20% (w/v) PEG 8000 and 0.1 M Tris-HCl, pH 8.5, at room temperature. After growth, crystals were stabilized by progressively increasing the PEG 8000 concentration up to 25 % (w/v). The crystals belonged to space group $P2_12_12_1$ and contained three tetramers of azurin per asymmetric unit (one tetramer consists of two azurin dimers). The BMMEdim was crystallized by the same method using a protein concentration of 15 mg ml^{-1} and a reservoir buffer containing 20% (w/v) PEG 2000 monomethyl ether, 0.01 M nickel chloride and 0.1 M Tris-HCl, pH 9.0. The crystals were hexagonal bipyramids belonging to spacegroup $P6_122$ and contained a single azurin dimer molecule per asymmetric unit. Data were collected on beamline BW6 at DESY, Hamburg, to limiting resolutions of 2.75 Å (SSdim) and 2.0 Å (BMMEdim). The refinement R-factors of the SSdim are rather high due to disorder of two monomers (chain F and K). In the BMMEdim, a BMME molecule links two azurin molecules across a crystallographic two-fold axis; therefore, this data set was refined in spacegroup $P6_1$ with a full dimer in the asymmetric unit and a slightly disordered BMME molecule connecting both monomers. Molecular replacement was carried out using AMoRe[23], the structures were refined using CNS[24] and model building was done in O[25]. Solvent accessible surface area was calculated by using NACCESS[26]. Van der Waals contacts were defined as interatomic separations between 3.2 and 4.0 Å. Crystallographic statistics are summarized in Table 2.

Determination of ρ. For the calculation of ρ, the ET Rates package[17] kindly provided by P.L. Dutton and coworkers was used. The cofactors were defined as the coppers plus the liganded atoms Sγ (Cys 112), Nδ1 (His 46 and His 117), Sδ (Met 121) and the backbone oxygen of Gly 45. For the SSdim, a standard value of ρ (0.75) was used because the intervening medium between the cofactors is ill defined and does not allow for precise determination of ρ.

Coordinates. Coordinates have been deposited in the Protein Data Bank (accession codes 1JVO for the disulfide dimer of N42C azurin and 1JVL for the BMME-linked dimer of N42C azurin).

Acknowledgments

We thank M.Ph. Verbeet and L.J.C. Jeuken for their help with the mutagenesis, C. Erkelens for his technical assistance during NMR measurements, A.D. Bain for his advice in using the MEX/MEXICO programs, C.C. Moser and P.L. Dutton for providing the ET Rates software and I.V. Kurnikov for his help in using the HARLEM program. This work is supported in part by grants of the EU, the National Research Council of Italy (to A.Mer., D.C. and G.R.) and the Deutsche Forschungsgemeinschaft (to O.E. and A.Mes.).

Correspondence should be addressed to G.W.C. *email: canters@chem.leidenuniv.nl*

Received 18 July, 2001; accepted 6 November, 2001.

1. Bendall, D.S. In *Protein electron transfer* (ed. Bendall, D.S.) 43–68 (Bios Scientific Publishers, Oxford; 1996).
2. Castro, G., Boswell, C.A. & Northrup, S.H. *J. Biomol. Struct. Dyn.* **16**, 413–424 (1998).
3. Liang, Z.X., Nocek, J.M., Kurnikov, I.V., Beratan, D.N. & Hoffman, B.M. *J. Am. Chem. Soc.* **122**, 3552–3553 (2000).
4. Nocek, J.M. *et al. Chem. Rev.* **96**, 2459–2489 (1996).
5. Ubbink, M. & Bendall, D.S. *Biochemistry* **36**, 6326–6335 (1997).
6. Qin, L. & Kostic, N.M. *Biochemistry* **32**, 6073–6080 (1993).
7. Hippler, M., Drepper, F., Haehnel, W. & Rochaix, J.D. *Proc. Natl. Acad. Sci. USA* **95**, 7339–7344 (1998).
8. Malatesta, F. *et al. Biochem. J.* **315**, 909–916 (1996).
9. Peerey, L.M., Brothers, H.M., Hazzard, J.T., Tollin, G. & Kostic, N.M. *Biochemistry* **30**, 9297–9304 (1991).
10. Nar, H., Messerschmidt, A., Huber, R., van de Kamp, M. & Canters, G.W. *J. Mol. Biol.* **221**, 765–772 (1991).
11. Nar, H., Messerschmidt, A., Huber, R., van de Kamp, M. & Canters, G.W. *J. Mol. Biol.* **218**, 427–447 (1991).
12. Mikkelsen, K.V., Skov, L.K., Nar, H. & Farver, O. *Proc. Natl. Acad. Sci. USA* **90**, 5443–5445 (1993).
13. van de Kamp, M., Floris, R., Hali, F.C. & Canters, G.W. *J. Am. Chem. Soc.* **112**, 907–908 (1990).
14. van Amsterdam, I.M. C. *et al. Chem. Eur. J.* **7**, 2398–2406 (2001).
15. Canters, G.W., Hill, H.A.O., Kitchen, N.A. & Adman, E.T. *J. Magn. Reson.* **57**, 1–23 (1984).
16. Bain, A.D. & Duns, G.J. *Can. J. Chem.* **74**, 819–824 (1996).
17. Page, C C., Moser, C.C., Chen, X. & Dutton, P.L. *Nature* **402**, 47–52 (1999).
18. Beratan, D.N. & Onuchic, J.N. In *Biological electron transfer.* (ed. Bendall, D.S.) 23–42 (Bios Scientific Publishers, Oxford; 1996).
19. Gray, H.B., Malmström, B.G. & Williams, R.J.P. *J. Biol. Inorg. Chem.* **5**, 551–559 (2000).
20. Kurnikov, I.V., Wenzel, W. & Beratan, D.N. HARLEM *http://www.kurnikov.org/harlem_main.html* (Biomolecular Modeling package, University of Pittsburgh; 2000)
21. Ponce, A., Gray, H.B. & Winkler, J.R. *J. Am. Chem. Soc.* **122**, 8187–8191 (2000).
22. Tezcan, F.A., Crane, B.R., Winkler, J.R. & Gray, H.B. *Proc. Natl. Acad. Sci. USA* **98**, 5002–5006 (2001).
23. Navaza, J. *Acta Crystallogr. A* **50**, 157–163 (1994).
24. Brünger, A.T. *et al. Acta Crystallogr. D* **54**, 905–921 (1998).
25. Jones, T.A., Zhou, J.Y., Cowan, S.W. & Kjeldgaard, M. *Acta Crystallogr. A* **47**, 110–119 (1991).
26. Hubbard, S.J. & Thornton, J.M. *NACCESS* (Department of Biochemistry and Molecular Biology, University College London; 1993).
27. Kraulis, P. J. *J. Appl. Crystallogr.* **24**, 946–950 (1991).
28. Esnouf, R. M. *J. Mol. Graph. Model.* **15**, 132–& (1997).
29. Merritt, E. A. & Bacon, D. J. *Methods Enzymol.* 277, 505–524 (1997).
30. DeLano, W.L. The PyMOL Molecular Graphics System. *http://pymol.sourceforge.net/* (DeLano Scientific, San Carlos, California; 2001)

© 2002 Nature Publishing Group http://structbio.nature.com